Abéngozar, M.A. et al. (2012) 'Blocking ephrinB2 with highly specific antibodies inhibits angiogenesis, lymphangiogenesis, and tumor growth', Blood, 119(19), pp. 4565–4576.

Available at https://doi.org/10.1182/blood-2011-09-380006

Blocking ephrinB2 with highly specific antibodies inhibits angiogenesis, lymphangiogenesis, and tumor growth

María Angeles Abéngozar,[1] Sergio de Frutos,[2] Sergio Ferreiro,[3] Joaquím Soriano,[4] Manuel Perez-Martinez,[4] David Olmeda,[5] Marco Marenchino,[6] Marta Cañamero,[7] Sagrario Ortega,[5] Diego Megias,[4] Antonio Rodriguez,[2] and Jorge L. Martínez-Torrecuadrada[1]

[1]Proteomics Unit, Biotechnology Programme, Centro Nacional de Investigaciones Oncológicas (CNIO), Madrid, Spain; [2]Molecular Biology Department, Faculty of Science, Universidad Autónoma de Madrid, Madrid, Spain; [3]Animal Facility, CNIO, Madrid, Spain; [4]Confocal Microscopy Unit, Biotechnology Programme, CNIO, Madrid, Spain; [5]Transgenic Mice Unit, Biotechnology Programme, CNIO, Madrid, Spain; [6]Spectroscopy and Nuclear Magnetic Resonance Unit, Structural Biology and Biocomputing Programme, CNIO, Madrid, Spain; and [7]Comparative Pathology Unit, Biotechnology Programme, CNIO, Madrid, Spain

Membrane-anchored ephrinB2 and its receptor EphB4 are involved in the formation of blood and lymphatic vessels in normal and pathologic conditions. Eph/ephrin activation requires cell-cell interactions and leads to bidirectional signaling pathways in both ligand- and receptor-expressing cells. To investigate the functional consequences of blocking ephrinB2 activity, 2 highly specific human single-chain Fv (scFv) Ab fragments against ephrinB2 were generated and characterized. Both Ab fragments suppressed endothelial cell migration and tube formation in vitro in response to VEGF and provoked abnormal cell motility and actin cytoskeleton alterations in isolated endothelial cells. As only one of them (B11) competed for binding of ephrinB2 to EphB4, these data suggest an EphB-receptor–independent blocking mechanism. Anti-ephrinB2 therapy reduced VEGF-induced neovascularization in a mouse Matrigel plug assay. Moreover, systemic administration of ephrinB2-blocking Abs caused a drastic reduction in the number of blood and lymphatic vessels in xenografted mice and a concomitant reduction in tumor growth. Our results show for the first time that specific Ab-based ephrinB2 targeting may represent an effective therapeutic strategy to be used as an alternative or in combination with existing antiangiogenic drugs for treating patients with cancer and other angiogenesis-related diseases. (*Blood*. 2012;119(19):4565-4576)

Introduction

Angiogenesis and lymphangiogenesis are highly complex coordinated processes through which new blood and lymphatic vessels, respectively, arise from preexisting ones.[1,2] Angiogenesis occurs physiologically during embryonic development, tissue repair (ie, wound healing), and menstruation, but it is also important in the pathogenesis of many diseases such as tumor growth and metastasis.[3] Because most tumors cannot grow and disseminate in the absence of new blood vessel formation, inhibition of the signaling pathways underlying pathologic angiogenesis is an important potential target for anticancer therapy.[4] The process of lymphangiogenesis is less well understood, however, the mechanisms regulating development and growth of lymphatic vessels have recently emerged as a very interesting field in cancer research, as they represent an important venue for metastatic dissemination.[5]

The well-established role of VEGF in promoting tumor angiogenesis has led to the development of therapeutic agents, including engineered mAbs and small molecule inhibitors such as bevacizumab (Avastin), sunitinib, and sorafenib[6-8] which selectively target VEGF/VEGF receptor pathways and have demonstrated promising clinical utility in treating solid neoplasms.[9] However, these VEGF-based treatments may result in only transient clinical benefits and tumors eventually develop a resistance to therapy and may exhibit a progression to greater malignancy.[10] Therefore, there is an urgent need to develop new agents targeting other pathways involved in angiogenesis that could be translated into more robust therapeutic outcomes to replace or complement existing therapies. A group of signaling molecules, the ephrins and their receptors (Eph), has recently emerged as attractive therapeutic targets because their pathways play critical roles in the development and maturation of the blood and lymphatic vascular systems.[11,12]

Eph receptor tyrosine kinases and their ligands, ephrins, control several cellular functions such as cell migration and cytoskeletal organization.[13,14] Ephrins are a family of cell-surface proteins linked to the cell membrane either by a GPI anchor (class A) or by a single transmembrane segment (class B). They act as activating ligands for the Eph receptors, which are divided into 2 classes depending on the ephrins with which they interact, although limited crosstalk between both classes has also been described.[15] An intriguing feature of Eph-ephrin signaling is that both, receptors and ligands, are able to transduce a downstream signaling cascade on interaction, resulting in bidirectional cell-to-cell communication. Eph-activated signaling is termed "forward" and ephrin-activated signaling is named "reverse." Eph receptors initiate forward signal transduction by autophosphorylation of several tyrosine residues located in the cytoplasmic part of the molecule in response to binding of clustered and membrane-attached ephrin ligands on adjacent cells. The reverse signaling activity is mediated by the C-terminal region of ephrins, which contains conserved

Submitted September 15, 2011;

tyrosines susceptible to phosphorylation[16] and a PDZ-binding domain, which can recruit PDZ domain-containing proteins on phosphorylation.[17] In addition, recent evidence has highlighted the importance of processes such as endocytosis of Eph/ephrin molecules coupled to the internalization of cell type-specific molecules with specialized functional roles such as AMPA receptors in neurons[18] or VEGF receptors in endothelial cells.[19,20]

In the blood vasculature, ephrinB2 is expressed on arterial angioblasts, endothelial cells (ECs) and perivascular mesenchymal cells, whereas one of its binding partners, the receptor EphB4, is specific of venous ECs.[21] Targeted inactivation of either *EphB4* or *EfnB2* genes in mice leads to failure of embryonic vessel formation and early lethality, demonstrating their critical role during physiologic angiogenesis.[22,23] This role of ephrinB2 also extends to tumor-derived angiogenesis and tumor growth.[19,24] Moreover, ephrinB2 controls lymphangiogenesis[20] and it has been recently shown that an ephrinB2 blocking peptide was able to suppress VEGF-induced lymphatic endothelial sprouting.[25] The development and remodeling of the lymphatic vasculature have been reported to be regulated through interactions mediated by its PDZ-binding domain[12]; this domain is also involved in the regulation of endothelial cell motility.[26]

Because the EphB4/ephrinB2 signaling is important in angiogenesis, hampering this protein-protein interaction could have several potential medical applications in angiogenesis-based diseases such as in tumor growth and metastasis. In fact, several groups have demonstrated that the monomeric soluble extracellular domain of EphB4 is able to block ephrinB2 interaction with its receptor, leading to inhibition of angiogenesis and tumor growth.[27,28] Here, we bring for the first time the proof of concept of the antiangiogenic efficacy of blocking ephrinB2 with highly specific human Abs in vitro and in vivo, showing a potent antitumor activity in different human cancer xenografts models in mice, which might have potential therapeutic applications.

Methods

Selection, production, and purification of anti-ephrinB2 scFv Abs

All experimental procedures were performed in accordance with institutional animal welfare guidelines and approved by the Research Ethics and Animal Welfare Committee of the Instituto de Salud Carlos III. Human phage Ab libraries were used for panning as previously described.[29] The recombinant extracellular region of human ephrinB2 fused to Fc domain of human IgG was used as the Ag source. This chimera was overexpressed by transient transfection of HEK293-EBNA cells using linear polyethylenimine (PEI; Polysciences) as the transfection reagent and purified from culture medium by affinity chromatography using protein A columns (GE Healthcare) on an ÄKTA system (GE Healthcare). Unique and specific soluble scFvs were identified by ELISA and DNA sequencing.

The expression and purification of His- and c-myc–tagged scFvs from selected bacterial clones were carried out as previously described.[29] Endotoxin was removed from purified scFvs, using polymixin B-based Detoxi-Gel Endotoxin Removing Gel (Thermo Scientific) according to the manufacturer's instructions. The eluted fractions were assayed for endotoxin content by using the Limulus Amebocyte Lysate (LAL) QCL-1000 kit (Lonza).

Endothelial cell tube formation assay

Ninety-six–well plates were coated with 50 jLL/well Matrigel (BD Biosciences) which was allowed to solidify at 37°C for 30 minutes, according to the manufacturer's instructions. HUVECs were detached with 100mM EDTA, washed twice in PBS, and resuspended in medium supplemented with 10% FBS. The cell suspensions were preincubated with 100 jLg/mL specific scFvs or controls for 15 minutes and plated onto the surface of the polymerized Matrigel (1.5×10^4 cells/well). After 6-hour incubation at 37°C, 5% CO_2, triplicate pictures were taken for each well using an inverted phase contrast microscope (Nikon). The number and length of the cord-like structures were measured in randomly selected fields.

Cell migration assays

Cell invasion was tested in transwell Boyden chambers with a gelatin-coated polycarbonated filter (8-jLm pore size, 0.1% w/v gelatin; Corning Life Sciences). A total of 1×10^5 cells were plated into the upper (pre-filter) well compartment containing 100 jLL of complete medium supplemented with 0.5% FBS, in the absence or presence of scFv (100 jLg/mL = 3jLM) and/or EphB4-Fc (2.5 jLg/mL; R&D Systems). Lower (postfilter) well compartment were filled with complete medium supplemented with 10% FBS as a cell attractant. After a 48-hour incubation period at 37°C, 5% CO_2, media were removed and cells were fixed with 4% paraformaldehyde (PFA) in PBS for 10 minutes at room temperature, and were then stained with 1 mg/mL DAPI (4'-6-diamino-2-phenylindole) for 10 minutes. Finally, cell invasion was analyzed by DAPI-positive nucleus counting at the top and the bottom of the chamber's filter using a Leica TCS SP5 confocal microscope equipped with a resonant scanner, a dry 20× Plan Apochromatic, 0.7 AN objective, and Leica LAS AF (Version 2.4.1) for image capturing, and the Imaris software (Bitplane) for image analysis.

Cell migration in scratch assays was also tested. Cells were grown to confluence in 24-well plates. After 1-hour incubation with starving media (0.5% FBS), culture dishes were scratched with a pipette tip and cells were then incubated in the absence or presence of 100 jLg/mL of the corresponding scFv using 100 ng/mL VEGF (PeproTech) as proangiogenic stimulus. The rate of wound closure was calculated by capturing images over a 24-hour period using a Leica AF6000 Workstation equipped with a dry 10× Plan Apochromatic, 0.4 AN objective, a Hamamatsu ORCA-AG CCD camera and Leica LAS AF software (Version 2.4.1). Lateral migration was measured as percentage of migrated area from time 0 to 24 hours using the Leica LAS AF software.

Random motility assays

Enhanced GFP (EGFP)–transfected HUVECs were treated with 100 jLg/mL of the corresponding scFv or left untreated as control in complete medium for 24 hours at 37°C, 5% CO_2. After Ab addition, the recording was started by acquiring fluorescence images every 10 minutes using a Leica AF6000 Workstation equipped with a dry 10× Plan Apochromatic, 0.4 AN objective, a Hamamatsu ORCA-AG CCD camera, and Leica LAS AF software (Version 2.4.1). Cell tracking analysis and statistics were performed with Imaris software (Bitplane).

Murine Matrigel plug angiogenesis assay

To test whether ephrinB2-specific scFvs were able to target neovasculature, growth factor–depleted Matrigel (BD Biosciences) in liquid form at 4°C was supplemented with heparin (6.6 jLg/mL) and VEGF (250 ng/mL) and was injected subcutaneously into the thoracic area of anesthetized 6-week-old female *nu/nu* mice. EphrinB2-specific scFvs and an irrelevant scFv were labeled with Alexa Fluor 750 by using the SAIVI Rapid Antibody Kit (Invitrogen Life Technologies) following the manufacturer's instructions. On day 5, when vasculature was macroscopically observed, mice were injected IV with 100 jLg of each Alexa 750–labeled scFv. Eight hours after injection, animals were killed, plugs were excised, and briefly stored at 4°C in PBS with 5% FBS before imaging acquisition. Fluorescence signal on plugs was acquired using an IVIS-200 small animal imaging system (Caliper Life Sciences).

To study the antiangiogenic capability of ephrinB2-specific scFvs, Matrigel plugs were implanted subcutaneously in nude mice as described in this section, and groups of 6 animals each were treated intravenously with a total dose of 15 mg/kg of specific and irrelevant scFvs distributed in 3 injections over a period of 10 days. Groups of mice were also inoculated

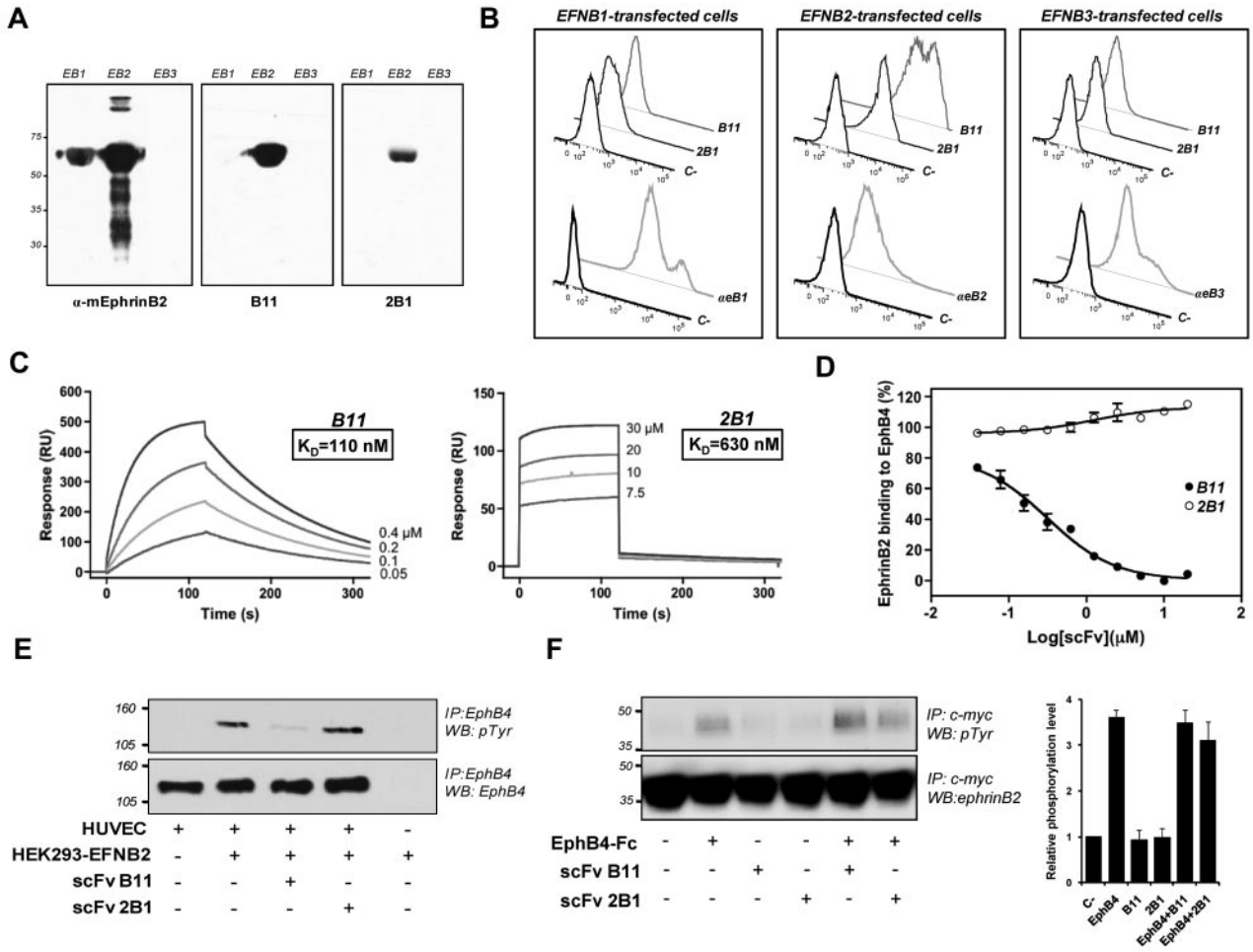

Figure 1. Characterization of selected ephrinB2-specific scFvs. (A) Specificity of scFvs for human ephrinB2-Fc (EB2) but not for other related members of the protein family, mouse ephrinB1-Fc (EB1) and human ephrinB3-Fc (EB3) by Western blot. Commercial anti–mouse ephrinB2 polyclonal Ab was used as control. (B) Flow cytometric analysis showing the specificity of B11 and 2B1 to ephrinB2 in native form. HEK293T cells overexpressing human ephrinB1 (left panel), ephrinB2 (middle panel), or ephrinB3 (right panel) were subjected to flow cytometry for detection of B11 and 2B1 binding. As positive controls, specific antisera of each member of the ephrinB family (aeB1, aeB2, and aeB3) were used (lower histograms of each panel). Incubations omitting the specific Abs were used as negative controls. (C) SPR sensorgrams of ephrinB2-specific scFvs, B11 on the left panel and 2B1 on the right, binding to immobilized ephrinB2-Fc are shown. The sensograms were corrected for response differences between the active and reference flow cells. EphrinB2-Fc was immobilized on CM5 chips and scFvs were passed over at concentration ranges noted on each sensorgram, giving affinity constants (K_D) of 110nM for B11 and 630nM for 2B1. (D) Inhibition assays using SPR for detection of bound ephrinB2. Serial dilutions of scFv B11 (F) or 2B1 (E) were mixed with 0.2jLM ephrinB2-Fc and injected over an immobilized sEphB4 on a CM5 chip. The relative amount of ephrinB2 binding to sEphB4 was measured immediately after injection of each sample and plotted as a function of scFv concentration. Mean values are shown with error bars indicating the SD (n = 3). (E) Activation of EphB4 receptor by tyrosine phosphorylation in HUVECs as a response to interaction with membrane-bound ephrinB2 in the absence or presence of ephrinB2-specific scFv in a cell-based assay. HEK293T cells overexpressing ephrinB2 were overlaid on HUVE cells with or without the corresponding scFv. Total (bottom panel) and phosphorylated EphB4s (top panel) after immunoprecipitation (IP) by Western blot (WB) with the respective Abs are shown. (F) Analysis of EphB4-induced ephrinB2 tyrosine phosphorylation in the absence or presence of B11 and 2B1. HEK293T cells transfected with c-myc–tagged ephrinB2 were treated as indicated and the corresponding cell extracts were immunoprecipitated with anti-c-myc Ab. Total (bottom panel) and phosphorylated (top panel) ephrinB2 were detected by Western blot. The graph on the right showed average levels of tyrosine-phosphorylated ephrinB2, quantified from 3 different immunoblotting experiments. Graph shows normalized results (means ± SD).

with Matrigel plugs supplemented with either vehicle (PBS) or VEGF (250 ng/mL) and left untreated as negative and positive controls, respectively. Then, Matrigel plugs were excised and divided into 2 parts: one was processed for IHC and the other part was used to determine hemoglobin concentration. For immunohistochemical analyses, plug pieces were fixed in 10% buffered formalin (Sigma-Aldrich), and embedded in paraffin. Identification of the endothelial cell population was carried out by CD34 staining with a specific rabbit mAb (Abcam) and counterstained with hematoxylin. Slides were scanned and images were captured and counted using the Carl Zeiss Mirax Scan and Axiovision 4.8 image processing system (Carl Zeiss MicroImaging). The other Matrigel blocks were homogenized in distilled water, spun at 13 000*g*, and supernatants were collected for hemoglobin measurement. Each supernatant was diluted 1:1 with TMB (3,3',5,5'-tetramethylbenzidine; Sigma-Aldrich) and optical densities at 620 nm were measured in a microplate reader (Bio-Rad). Values were normalized to the plug weight.

Tumor xenografts

Log-phase BxPC3 carcinoma pancreatic cells (1×10^6) in PBS were implanted subcutaneously into the flank of SCID mice on day 0. Tumors were measured 3 times a week using a caliper, and tumor volume was calculated using the formula: $V = \text{length} \times (\text{width})^2 \times 0.5$. When the mean tumor volume reached = 30 mm^3, mice were randomized into groups of 10 and were treated with IV injections of B11 or 2B1 diluted in 0.2 mL of PBS once every other day until reaching a total dose of 20 mg/kg. Control animals were given vehicle (PBS) alone. Tumor sizes were monitored at least twice a week. SW620 colon carcinoma (5×10^6) or H460 lung carcinoma (5×10^6) cells stably expressing mCherry were subcutaneously injected in the back of female *nu/nu* mice (n = 4) on day 0. Treatment with B11 or 2B1 was initiated at day 4 following the schedule described in this section. Tumor size was followed by fluorescence imaging at 610 nm twice per week using an IVIS-200 small animal imaging system (Caliper Life

Table 1. Amino acid sequences of CDRs within the V_H and V_L regions from ephrinB2-specific scFv clones

scFv clones	CDR1	CDR2	CDR3
V_H			
A1	SYWIG	YPGDSDTRYGPSFQG	HPAAAGTHDGFDI
B11	DYYIH	WMNPSSGNTGYAQKFQGR	DITGTATGFDY
E4	SYAMH	VISYDGSNKYYADSVKGR	DYGGYRYGYFDY
2B1	DYAMH	GISWNSGSIGYADSVKGR	GHRTSDAFDI
V_L			
A1	TGSSSNIGAGYDVH	GNSNRPS	AAWDDSLNGL
B11	RSSQSLLHSNGYNYLD	GSNRAS	MQGLLSPVT
E4	TGGGSNIGAGHDVH	SNTNRP	QSYDSSLSGWV
2B1	GGDSIGLKSVH	SDSDRPS	QVWDSSSDHMV

CDR indicates complementarity determining region; V_H, heavy-chain V region; V_L, light-chain V region; and scFv, single-chain Fv.

Sciences) and photons emitted (represented as photons per second per square centimeter per steradian) from tumoral masses were quantified using Living Image software (Caliper Life Sciences).

More information on the methods and materials can be found in supplemental Methods (available on the *Blood* Web site; see the Supplemental Materials link at the top of the online article).

Results

Identification and characterization of human Abs against ephrinB2

We have developed anti-ephrinB2 human Abs using a phage display approach (Figure 1). A total of 29 ephrinB2 binders were identified by ELISA (supplemental Figure 1A) and 4 of them (A1, B11, E4, and 2B1 clones) were distinct as determined by DNA sequencing (Table 1). Two scFv clones, B11 and 2B1, were successfully produced in *Escherichia coli*. To exclude any possible complications from bacterial endotoxins, we used polymyxin B affinity chromatography to remove them from the purified scFv preparations (endotoxin level < 0.05 EU/mL).

The selected scFvs were highly specific for ephrinB2 as they reacted with this ligand, but not with other related members of the protein family, measured by Western blot, flow cytometry, and ELISA (Figure 1A-B, and supplemental Figure 1C). Surface plasmon resonance (SPR) analysis indicated that the binding affinity constant (K_D) of B11 and 2B1 were 110nM and 630nM, respectively (Figure 1C). Next, we determined the ability of these Abs to compete for binding to ephrinB2 with its natural receptor EphB4 by SPR. As shown in Figure 1D, B11 led to a significant dose-dependent decrease in the binding of ephrinB2 to EphB4 ($IC_{50} = 0.3$jLM), while no blocking effect was found for 2B1 over the experimental concentration range. Likewise, B11 was able to block membrane-bound ephrinB2-induced EphB4 phosphorylation in a cell-based assay; by contrast, 2B1 did not affect ephrinB2-induced EphB4 activation (Figure 1E). These results established that B11, but not 2B1, competes with EphB4 for binding to ephrinB2 and blocks EphB4 signaling in the context of cell-cell contact. The effect of B11 and 2B1 Abs on EphB4-induced ephrinB2 phosphorylation was also tested. We assessed the phosphorylation status of ephrinB2 in c-myc–tagged ephrinB2-transfected HEK293 cells, treated with combinations of clustered EphB4-Fc and each scFv. As shown in Figure 1F, EphB4-induced ephrinB2 phosphorylation was not significantly compromised by the presence of both scFvs indicating that B11 and 2B1 were not able to block ephrinB2-EphB4 interaction and receptor-induced phosphorylation of ephrinB2.

EphrinB2-specific Abs inhibit HUVEC migration and tube formation

The antiangiogenic activities of ephrinB2-specific Abs were tested in vitro (Figure 2). We first assessed the expression of ephrinB2 in endothelial cells (HUVECs). We found that HUVECs basal ephrinB2 expression was enhanced by VEGF treatment (supplemental Figure 2A). The selective binding of ephrinB2-specific scFvs to HUVECs, confirmed by FACS and immunofluorescence (supplemental Figure 2B-C), had no appreciable cytotoxic effects on HUVECs (supplemental Figure 2D).

To examine whether B11 and 2B1 scFvs affected the migratory capacity of endothelial cells, we performed transwell migration and wound healing assays. Transwell migration assays showed that in the presence of B11 and 2B1, the percentage of HUVEC migrated cells was reduced from 80% (untreated) to 50% and 40%, respectively (Figure 2A). In addition, activation of reverse ephrinB2 signaling by clustered EphB4-Fc slightly stimulated HUVEC migration with 95% of the migrating cell; however, ephrinB2-specific scFvs completely blocked EphB4-Fc–induced HUVEC migration. Moreover, ephrinB2-specific scFvs markedly inhibited the VEGF-induced lateral migration of HUVECs in wound healing assays, decreasing the percentage of migrated cells from $= 70\%$ (control/no scFv) to 25% in the presence of 3jLM B11 or to 30% of 3jLM 2B1, similar to that obtained in the absence of VEGF. As expected, HUVEC migration was not affected by an irrelevant scFv (Figure 2B).

We next carried out in vitro Matrigel assays to analyze the effect of B11 and 2B1 on HUVEC morphologic differentiation (Figure 2C). HUVEC treatment with either ephrinB2-specific scFvs significantly inhibited the formation of tube-like structures by $> 40\%$, inducing a sheet-like monolayer pattern. Overall, these results provided strong evidence of the antiangiogenic activity of ephrinB2-specific scFvs in vitro, affecting endothelial cell migration and tubulogenesis.

Effect of anti-ephrinB2 scFvs on single-cell random migration

To further analyze the effect of anti-ephrinB2 Abs on endothelial cell migration independent of cell-cell interactions, we studied single-cell random migration during 24 hours with treated and control HUVECs expressing EGFP by using fluorescence time-lapse video microscopy. We observed that B11-treated cells displayed altered motility in comparison with nontreated cells (Figure 3A, and supplemental Videos 1-3). They appeared to be poorly spread with numerous unstable lamellipodial protrusions and frequent changes in overall direction of movement. The migration pattern of 2B1-treated cells was also erratic, less pronounced though. By contrast, control cells appeared polarized,

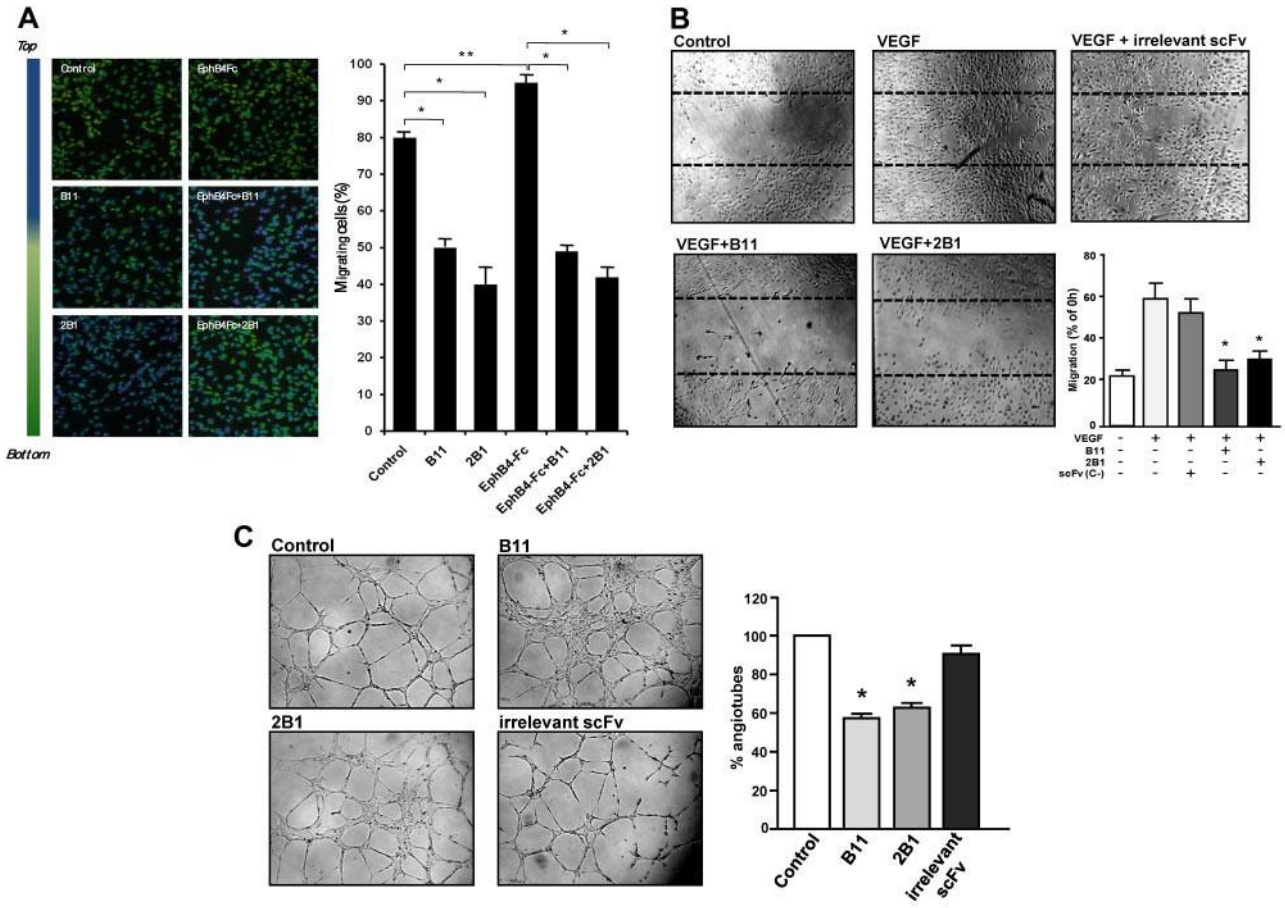

Figure 2. Characterization of antiangiogenic capability of ephrinB2-specific scFvs. (A) HUVEC migration (Transwell) assays in the absence or presence of B11 or 2B1 and/or clustered EphB4-Fc are shown. FBS in the bottom chamber was used as migration stimuli. Cells crossing the Transwell membrane are in green, whereas the blue signal indicates cells that remain at the upper compartment. Results are expressed as the percentage ± SD of migrated cells relative to total cells. *$P < .001$ and **$P < .01$ as determined by an unpaired Student *t* test. (B) Analysis of lateral migration of HUVECs by wound healing assays in vitro. HUVECs were grown to confluence when scratches were done. Cells were incubated with starving media in the absence (Control) or presence of 100 ng/mL VEGF as migrating stimulus. Cell migration was monitored over 24 hours with 100 jLg/mL ephrinB2-specific scFvs (B11 or 2B1) or an irrelevant scFv as indicated. Representative still photographs (4X magnification) taken 24 hours after scratching are shown (original wound areas at time 0 are indicated by dotted lines). Quantification of lateral migration after 24 hours is shown in the bottom right panel. Each scFv was assayed at least 3 times and the corresponding values (means ± SD) were represented as the percentage of migrated area from time 0. *$P < .01$ versus control. (C) Tubular formation assay. HUVECs were cultured on standard Matrigel in VEGF-stimulated conditions in the absence (control) or presence of anti-ephrinB2 (B11 or 2B1) scFvs or an irrelevant scFv. Representative microphotographs of tube formation after 6 hours of culture (4X magnification) are shown. Graph shows quantitative measure of tube formation. Each treatment was assayed at least 3 times, and the corresponding values (means ± SE) were plotted as percentages of tube formation in the respective condition. *$P < .001$ versus control.

exhibited more elongated cell shape and frequently continued migrating in the same direction without turning. Analysis of cell migration showed that B11-treated cells displayed a significantly reduced migration speed (Figure 3B) and they traveled a shorter accumulated distance (Figure 3C), with a reduction in the index of straightness defined as the ratio of the displacement of a cell to the accumulated distance (Figure 3D). 2B1-treated cells showed a smaller straightness index compared with control cells despite to display similar speed and migration length, indicating that only the cell directionality was affected.

Treatment with anti-ephrinB2 Abs leads to an increase in stress fibers

To assess whether these motility changes were coupled with cell morphology differences, we quantified cell shape changes by measuring the actin cytoskeleton (Figure 4). Anti-ephrinB2–treated cells adopted a more round cell-shape morphology, whereas control cells exhibited a more elongated phenotype (Figure 4A). Quantification of cell areas showed that the size of the cells treated with ephrinB2-specific scFvs was significantly reduced by 40% compared with control cells (Figure 4B). In addition, densitometry analysis of polymerized F-actin by fluorescence intensity showed that treatment with B11 increased significantly the number and thickness of cytoplasmic actin-containing stress fiber (Figure 4C) compared with the untreated cells, indicating that actin cytoskeleton dynamic was altered. 2B1 also induced actin stress fibers, albeit to a lesser extent than B11.

Impairment of VEGF-induced Matrigel angiogenesis in vivo by anti-ephrinB2 scFvs

The antiangiogenic properties of anti-ephrinB2 Abs in vivo were analyzed by Matrigel plug assays in athymic nude mice. First, we tested the ability of the anti-ephrinB2 scFvs to properly target neovascularization developed within the VEGF-supplemented Matrigel (Figure 5A). Strong fluorescent signals were detected in the Matrigel plugs from animals treated with Alexa 750–labeled B11, whereas mice injected with the 2B1–Alexa 750 conjugate showed only moderate fluorescence intensities, indicating that

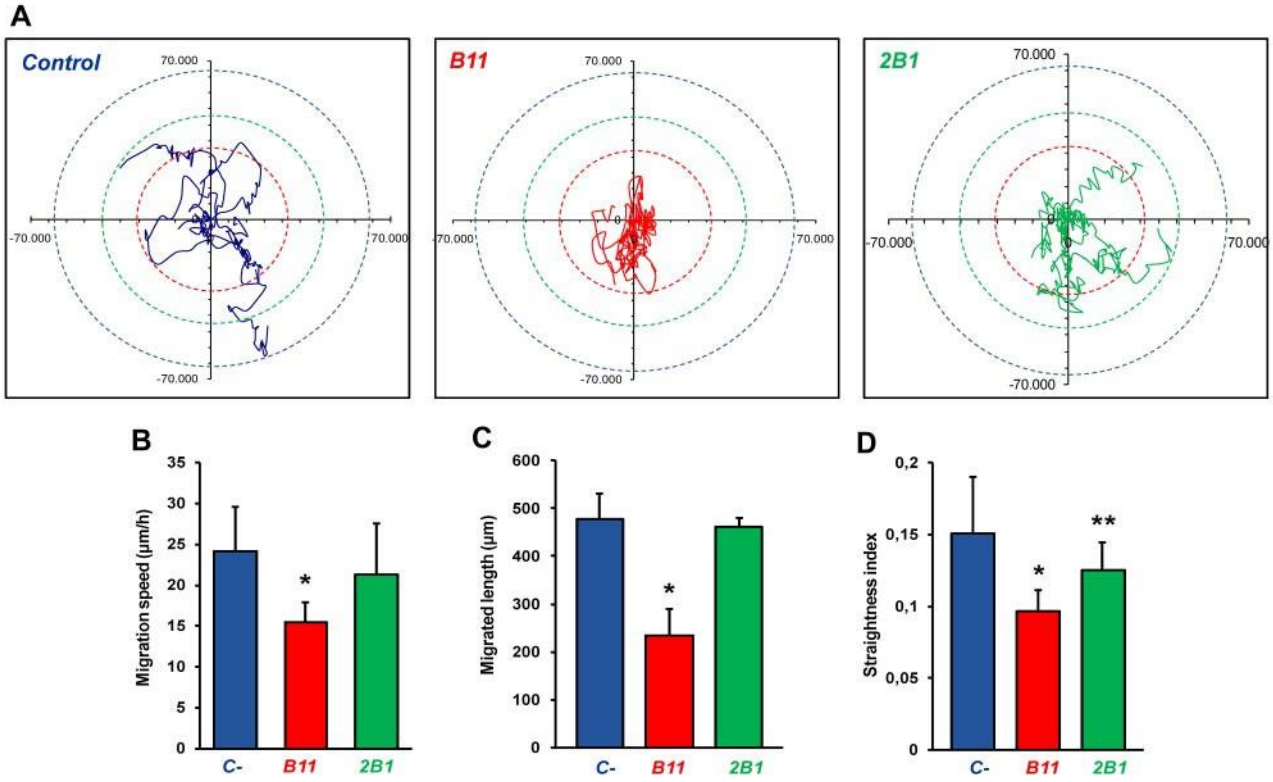

Figure 3. Effect of ephrinB2-specific scFvs on single-cell random migration. Cell tracking analysis was carried out for 24 hours at a rate of 1 frame per 10 minutes. Several parameters of random motility were quantified on EGFP-transfected HUVEC culture: (A) 5 significant tracks of untreated, B11-, and 2B1-treated cells were plotted in blue, red, and green, respectively. Trajectories of each group of cells were standardized because they all begin at the same starting post. Colored dotted circles represent the maximum distance covered by a group of cells within 24 hours. (B) The speed of treated and untreated cells (jLm/h). (C) The total length migrated by treated and untreated cells (jLm) and (D) directionality scored as straightness index (distance from the origin/total distance ratio). n = 17, *$P < .001$, and **$P < .05$ versus untreated control cells.

B11 targeted neovessels more efficiently than 2B1. We next analyzed their effect on angiogenesis. After Matrigel implantation, animals were treated intravenously with a total dose of 15 mg/kg body weight of anti-ephrinB2 scFvs or an irrelevant scFv. After 10 days, the Matrigel plugs were removed and the number of neovessels was quantified by CD34 immunostaining and hematoxylin counterstaining (Figure 5C). Very few blood vessels were present in the B11-treated VEGF plugs, similar to those observed in the absence of growth factors. An extensive amount of vessels was detected in the VEGF plugs either untreated or treated with an irrelevant scFv. A scanty pattern of endothelial structures was observed in the VEGF plugs treated with 2B1.

The hemoglobin content of the Matrigel plugs was also measured to quantify functional vessel recruitment. Hemoglobin amount within the VEGF-supplemented plugs from B11-treated mice was drastically reduced compared with untreated or treated with an irrelevant scFv (Figure 5B), whereas the 2B1-treated plugs exhibited a moderate but still significant reduction in hemoglobin content. Taken together, these results suggest that anti-ephrinB2 scFvs, B11 and 2B1 (albeit at a lower extent), were able to inhibit efficiently angiogenesis and functional blood vessel formation in vivo.

Anti-ephrinB2 scFvs inhibits tumor xenograft growth

We further examined the inhibitory capacity of anti-ephrinB2 scFvs on tumor growth in nude or SCID mice bearing subcutaneous human tumor cell xenografts (Figures 6-7). First, we quantified the ephrinB2 mRNA expressed in the carcinoma cells used (BxPC3, pancreas; SW620, colon; and H460, lung). Our results indicated that SW620 cells expressed the highest levels of ephrinB2 mRNA, followed by BxPC3 cells with a moderate expression and finally H460 with very low levels of ephrinB2 mRNA (supplemental Figure 3A). Subsequent immunohistochemical analysis of xenograft tissue sections confirmed those ephrinB2 expression levels observed at mRNA level and a vascular ephrinB2 expression pattern in all xenografts tested (supplemental Figure 3B). Furthermore, to study whether the treatment with anti-ephrinB2 Abs could directly affect to the tumor cell proliferation and survival, these carcinoma cell lines were cultured in the presence of different Ab concentrations. No direct effect on tumor cell growth was observed in vitro in any of the cell lines at the concentrations tested (supplemental Figure 3B).

To evaluate the biodistribution, tumor vascular-targeting capability and circulation time of anti-ephrinB2 scFvs, we did in vivo targeting experiments using near-infrared (IR) fluorescence imaging (supplemental Figure 4). The B11 and 2B1 scFvs were fluorescently labeled and IV injected into mice bearing H460 tumors; this cancer cell line displayed the lowest level of ephrinB2, therefore most of the specific signal will come from the tumor vasculature rather than the tumor cell population. Both Abs showed selective accumulation in the tumors with peak signal intensities between 2 hours and 6 hours, albeit 2B1 exhibited a tumor uptake at a lower level than B11 (= 2.0-fold). The signal intensity decreased by 24 hours and remained detectable for at least 48 hours. Ab clearance via the kidneys and liver (data not shown) was observed throughout the experimental period (48 hours).

We first studied the effect of B11 and 2B1 on tumor growth by using BxPC3 cells in SCID mice. The Abs were well tolerated by

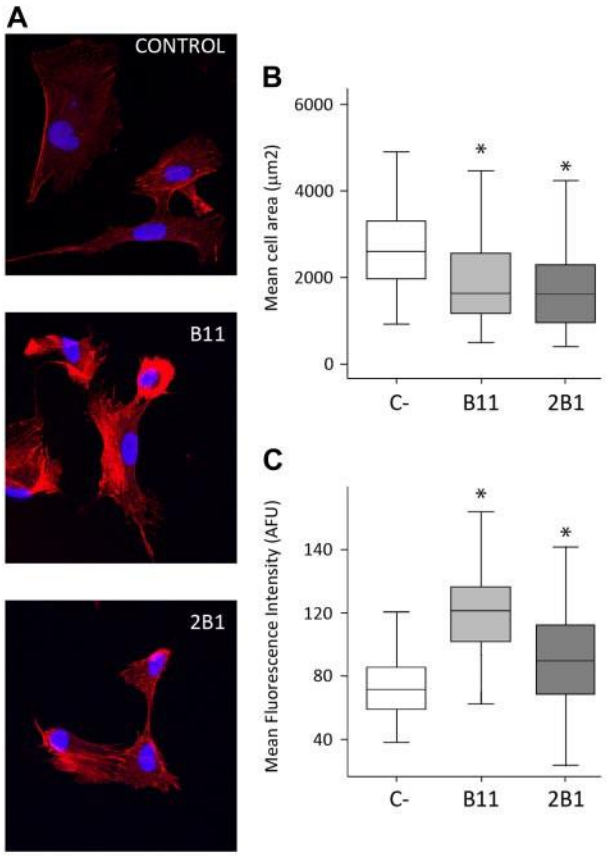

Figure 4. Increase of F-actin stress fibers by treatment with ephrinB2-specific scFvs. (A) Detection of polymerized actin was performed by staining with Alexa 568–labeled phalloidin on HUVEC cultures treated with B11, 2B1, or irrelevant scFv (C-) for 4 hours. (B) Cell area (jLm^2) and (C) fluorescence intensity (arbitrary fluorescence unit [AFU]) were quantified using Definiens Software XD Version 1.5 and were represented as the median of 150 cells (n = 150), upper and lower quartile, and upper and lower extreme for each group. *$P < .001$ versus control.

mice, with no detectable side effects. As shown in Figure 6A, B11 IV administration significantly inhibited tumor growth. The ratio of mean tumor volume of B11-treated mice over saline-treated control mice (T/C) after 30 days was 0.312, whereas 2B1-treated mice on the same schedule exhibited a moderate reduction with a T/C value of 0.638. To study the mechanisms underlying the observed tumor growth delay, an immunohistochemical study was carried out on tumors (25 after implantation) to analyze their apoptotic, proliferative, angiogenic, and lymphangiogenic status by staining for caspase-3–active, Ki67, CD34, and LYVE1, respectively (Figure 6B). The percentage of apoptotic cells increased around 5-fold in the B11-treated group, whereas treatment with 2B1 resulted in a lowest but still significant 2.5-fold increase. On the other hand, no significant differences were observed in tumor cell proliferation measured by Ki67 staining between treated and untreated mice. Immunohistochemical analyses using Abs against blood vascular endothelial marker CD34 revealed that the B11-treated tumors had significantly lower blood vessel density than control tumors, representing a reduction of 85%. Treatment with 2B1 also diminished the tumor vascularized area albeit at a slightly lower extent than B11 (63% reduction). Furthermore, we observed marked differences in vessel morphology (Figure 6C). In control tumors, the vasculature was mainly formed by tortuous and uneven vessels, with profuse branching and readily noticeable filopodial extensions. In contrast, the tumor blood vessels in anti-ephrinB2–treated mice showed clearly reduced-to-absent filopodial protrusions and a smoother appearance, with less branching.

Finally, tumor lymphatic vessel density was analyzed by LYVE1 staining. Anti-ephrinB2 treatment resulted in a dramatic reduction of the lymphatic vasculature, observed both in the tumor periphery and in the core of the treated tumors, particularly in those animals treated with B11, in which the presence of lymphatic vessels was almost completely inhibited.

We next decided to determine whether the antitumor activity of B11 and 2B1 observed in the BxPC3 model could be detected in other tumor models. Administration of B11 to mice bearing mCherry-expressing SW620 colon tumor or H460 lung tumor xenografts resulted in a strong tumor growth inhibition as measured by monitoring the far-red fluorescence at 610 nm (Figure 7). Compared with control tumors, SW620 and H460 xenografts showed an 85% and a 60% tumor reduction 23 days postimplantation. Tumor sections were further stained with anti-CD34 and anti-LYVE1 Abs; CD34 staining showed that the blood vessel density was drastically decreased in the treated tumors, with a reduction of = 85% compared with control tumors. Likewise, the B11-treated tumors almost lacked lymphatic vessels, as measured by levels of LYVE1 staining. Treatment with 2B1 decreased moderately SW620 and H460 tumor growths by 35% and 25%, respectively, relative to vehicle control. Quantification of vascular area density revealed a similar decrease in blood and lymphatic vessels of 50% and 75%, correspondingly, in both xenograft models.

Taken together, these results suggest that the antitumor effects exerted by the anti-ephrinB2 Abs were mediated by antiangiogenic and antilymphangiogenic mechanisms and that the observed tumor growth inhibition was not cancer cell type-specific and was independent of the levels of ephrinB2 expression in tumor cells.

Discussion

The critical role of ephrinB2-EphB4 in angiogenesis and lymphangiogenesis provides the rationale for developing therapeutic reagents aimed at interrupting these processes.[30,31] In addition, ephrinB2 has recently emerged as an attractive angiogenic target itself given that this protein has been shown to play an essential role in the function of VEGFR2 and VEGFR3 in driving angiogenesis and lymphangiogenesis.[19,20] Indeed, antagonizing EphB4-ephrinB2 binding seems to be effective in cancer-mediated angiogenesis from the therapeutic standpoint. Various molecules have been investigated for this purpose to date,[32,33] including a monomeric soluble extracellular domain of EphB4.[27,28,34] However, it has been described that EphB4 receptor interacts preferentially with ephrinB2 but it can also interact weakly with ephrinB1 and ephrinB3,[35] so the soluble EphB4 receptor might promiscuously bind to different ephrin ligands and, therefore, the precise target of such a therapeutic approach remains undefined. To achieve a selective and specific targeting of ephrinB2, we performed an Ab-based strategy. In the present work, we were evaluated the use of highly specific human Ab fragments (scFv) directed against ephrinB2 to interfere ephrinB2-EphB4 signalings as an immunotherapeutic strategy.

Angiogenesis and lymphangiogenesis are complex and tightly orchestrated multistep processes that involve several biologic systems such as cell proliferation, migration, and tube formation. Suppression at any step of these processes will inhibit the formation of new vessels. We have demonstrated antiangiogenic effects of the 2 selected ephrinB2-specific Abs (B11 and 2B1) in

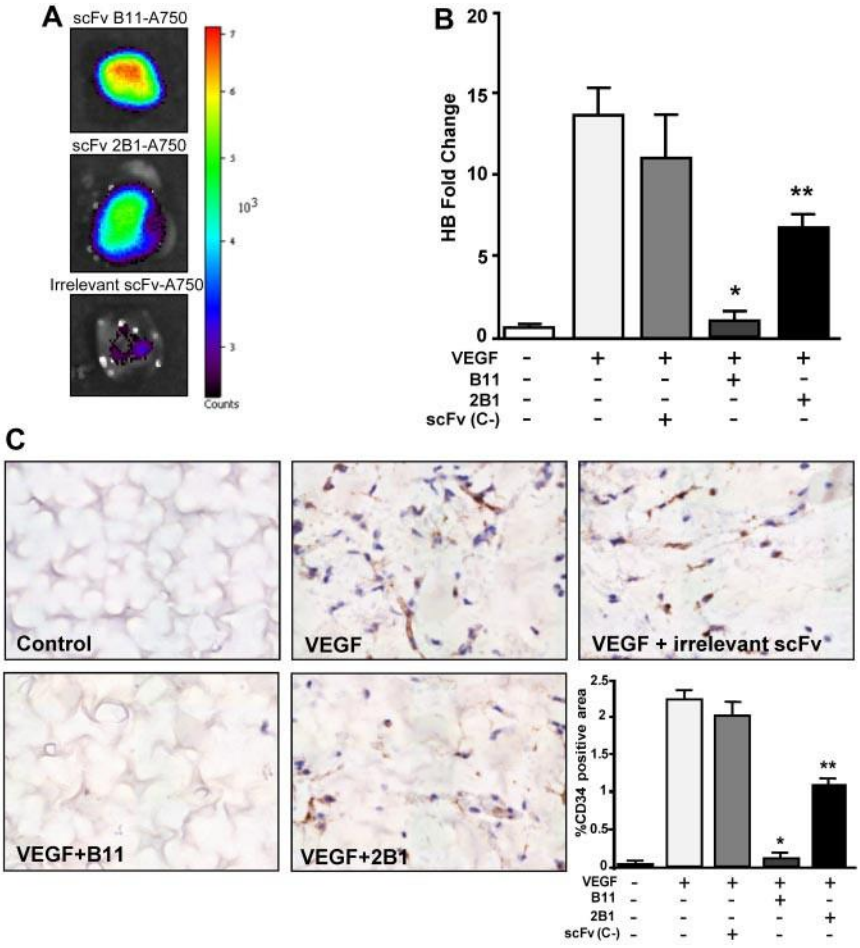

Figure 5. Inhibition of VEGF-induced neoangiogenesis in a Matrigel plug model. (A) In vivo assessment of the vascular targeting capability of ephrinB2-specific scFvs labeled with Alexa 750 in mice bearing VEGF-containing Matrigel plugs. Representative fluorescent images of Matrigel plugs taken from the killed mice at 8 hours after IV injection of Alexa 750–conjugated scFvB11 (top panel), Alexa 750–conjugated scFv2B1 (middle panel), or an irrelevant Alexa 750–conjugated scFv (bottom panel). Color-coded scale of fluorescence counts (X 10^3) is shown at right. (B) Quantification of hemoglobin in Matrigel plugs removed from the scFv-treated or untreated mice as indicated, after 10 days after implantation (n = 6). Data are presented as hemoglobin fold change over unstimulated and untreated group (negative control). *$P < .001$ and **$P < .01$ versus VEGF-stimulated and untreated positive control. (C) Representative sections of the indicated Matrigel plugs excised on day 10. Endothelial cells were labeled with CD34 (brown), and the sections were counterstained with hematoxylin (blue). Quantification of CD34-positive area is shown in the bottom right panel. Bars represent the mean percentage of positive area ± SD (n = 6). *$P < .001$ and **$P < .01$ versus VEGF-stimulated and untreated positive control.

vitro at 2 levels: inhibition of migration and tubular structure formation. Consistent with previously reported data,[36] we described that activation of reverse signaling by clustered EphB4-Fc resulted in an increased motility of endothelial cells. Interestingly, this effect was completely abolished by both Abs. In the case of B11, it blocks EphB4-ephrinB2 interaction, at least in part, by competing for receptor binding. However, the mechanism through which 2B1 blocks motility remains unknown as this Ab does not apparently interfere with EphB4-ephrinB2 interaction; this fact argues against a role of the EphB4 receptor in this process. Therefore, the exclusive inhibition of EphB4 activation does not completely explain the observed effects. Interestingly, EphB4-induced ephrinB2 phosphorylation was unaffected by the binding of both Abs, suggesting that the antiangiogenic effects appeared to be independent of ephrinB2 activation through tyrosine phosphorylation. Hence, it is possible that the anti-ephrinB2 Abs themselves may inhibit ephrinB2 activation by forcing it into a conformation that is not able to trigger the signal transduction cascade, just as the Ab binding could inhibit ligand oligomerization and clustering[37] or impair reverse signaling through PDZ interactions. Additional work will be needed to conclusively address the precise mechanisms of these function-blocking Abs.

To further demonstrate that some of the effects observed were receptor independent, EGFP-expressing endothelial cells were cultured at low density, so that ephrinB2 could not be substantially activated through a mechanism involving cell-cell contact. Single HUVECs treated with anti-ephrinB2 Abs in the absence of cell-cell interactions showed an abnormal morphology and motility compared with untreated cells, suggesting that ephrinB2 might function in a cell-autonomous fashion. Indeed, it has been recently described that ephrinB2 is able to modulate cellular motility and morphology independently of Eph-receptor binding in endothelial cells because blocking peptides or ephrinB2 mutations that abolish interaction with EphB4 did not lead to significant differences in motility behavior or cellular morphology.[26] Moreover, isolated ephrinB2-deficient cells presented morphologic changes consisting of insufficient spreading with many, but unstable lamellipodial protrusions and defects in motility (eg, disorganized migration with frequent changes of direction).[38] So, as the abnormalities observed in anti-ephrinB2-treated endothelial cells are similar to those described when the reverse signaling through the C-terminal PDZ-binding motif of ephrinB2 is impaired or ephrinB2 is not expressed, we speculate that the anti-ephrinB2 scFvs could block the Eph-independent functions of ephrinB2 leading to an aberrant motility that would impair the VEGF-driven angiogenic properties of endothelial cells. The fact that B11 was more efficient in hampering migration than 2B1 could be attributed to its higher affinity for ephrinB2. Also, because they recognize different epitopes of ephrinB2, the effectiveness of the blocking mechanism could be distinct.

In addition, the treatment with anti-ephrinB2 scFvs altered the actin cytoskeleton; consequently, the treated cells become more rigid, which may account for the inhibition of cellular motility. In contrast, the activation of ephrin-B reverse signaling has been shown to lead to actin stress fiber disassembly and cell migration.[39] The anti-ephrinB2–Ab-induced cell rigidity could also explain why treated cells formed epithelial sheets on the Matrigel instead of assembling into capillary-like tubular structure in a tube formation assay. This induction of stress fibers in migratory endothelial cells has also been described as the effect of a common mechanism

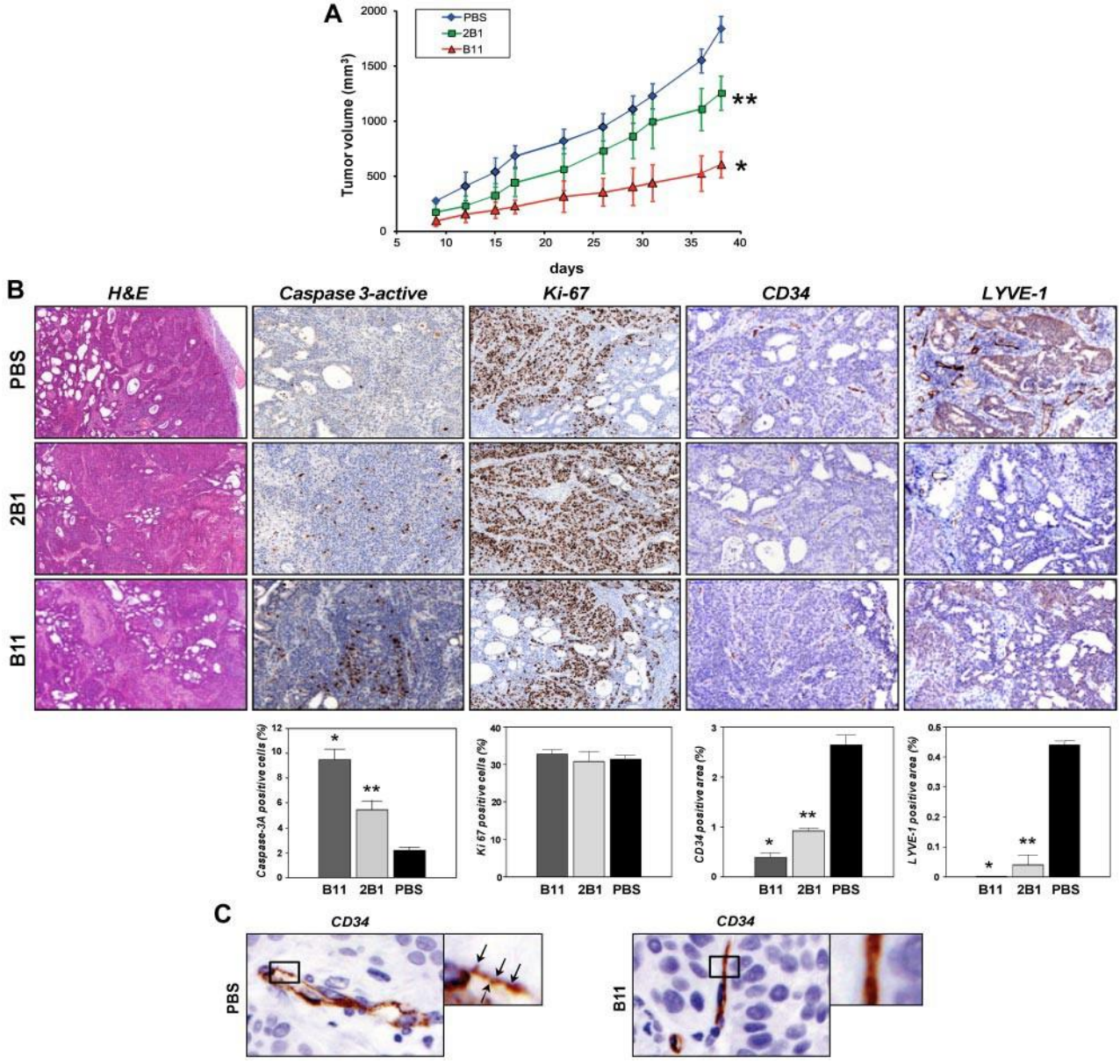

Figure 6. In vivo antitumor activity of the ephrinB2-specific scFvs on BxPC3 xenograft. (A) Groups of SCID mice (n = 10) bearing BxPC3 tumors were treated intravenously with either B11 or 2B1 at a total dose of 20 mg/kg or with an equal volume of PBS in alternating days starting when tumors were macroscopically noticeable. Tumor volumes were measured with calipers about twice a week and mean tumor volume was represented versus time for each group. Bars correspond to SD (*$P < .001$, **$P < .01$ versus PBS control). (B) BxPC3 tumor tissues excised on day 2 after treatments from mice injected with either PBS or 2B1 or B11 as indicated, were stained with H&E or by IHC using Abs anti-caspase 3–active to assess apoptosis (brown, apoptotic cells; magnification, 200X), anti-Ki67 to assess proliferation (brown, proliferating cells; magnification, 200X), anti-CD34 to evaluate blood vessel density (brown, endothelial cells; magnification, 200X), and anti-LYVE-1 to measure lymphatic vessel density (brown, lymphatic endothelial cells; magnification, 200X). Representative examples of tumor sections in each experimental condition are shown in the photographs. Results are shown as the percentages of the positive cells or areas relative to the total number of cells or areas quantified with the AxioVison software. Each data point is derived from 3 tumors and corresponds to the mean ± SD. *$P < .001$, **$P > .01$ versus PBS control. (C) Higher magnifications of CD34-positive blood vessels from BxPC3-bearing mice treated with PBS (left panel) or B11 (right panel). Arrowheads point to filopodial protrusions in untreated tumor vessels.

exerted by a panel of diverse angiogenesis inhibitors that induce the inhibition of cellular motility.[40]

A very important goal of this work was to investigate the therapeutic potential of the anti-ephrinB2 scFvs. We evaluated their impact on in vivo angiogenesis and found that physiologic angiogenesis was significantly inhibited, highlighting ephrinB2 as an important antiangiogenic target. The different scFv efficiency observed could be due to their distinct affinities; B11 has a higher affinity and target vascular network more efficiently than the 2B1. To explore their therapeutic antiangiogenic potentials, we tested whether anti-ephrinB2 Abs affected to pathologic angiogenesis, such as tumor angiogenesis, by using them in several xenograft human tumor models. Systemic treatment of mice bearing the BxPC3 pancreatic carcinoma cell line with anti-ephrinB2 scFvs resulted in an effective inhibition of tumor xenograft growth; again B11 yielded the most potent effects probably because of its higher affinity. Apoptosis was significantly increased in tumors from animals treated with anti-ephrinB2 Abs whereas cell proliferation was not affected; the increased apoptosis over similar proliferation rates may account for the observed reduction in tumor growth in treated mice. Tumor xenografts showed a dramatic reduction in the number of blood and lymphatic vessels, indicating that anti-ephrinB2 Abs mediated angiogenic and lymphangiogenic suppression. Similar results were obtained with other xenograft

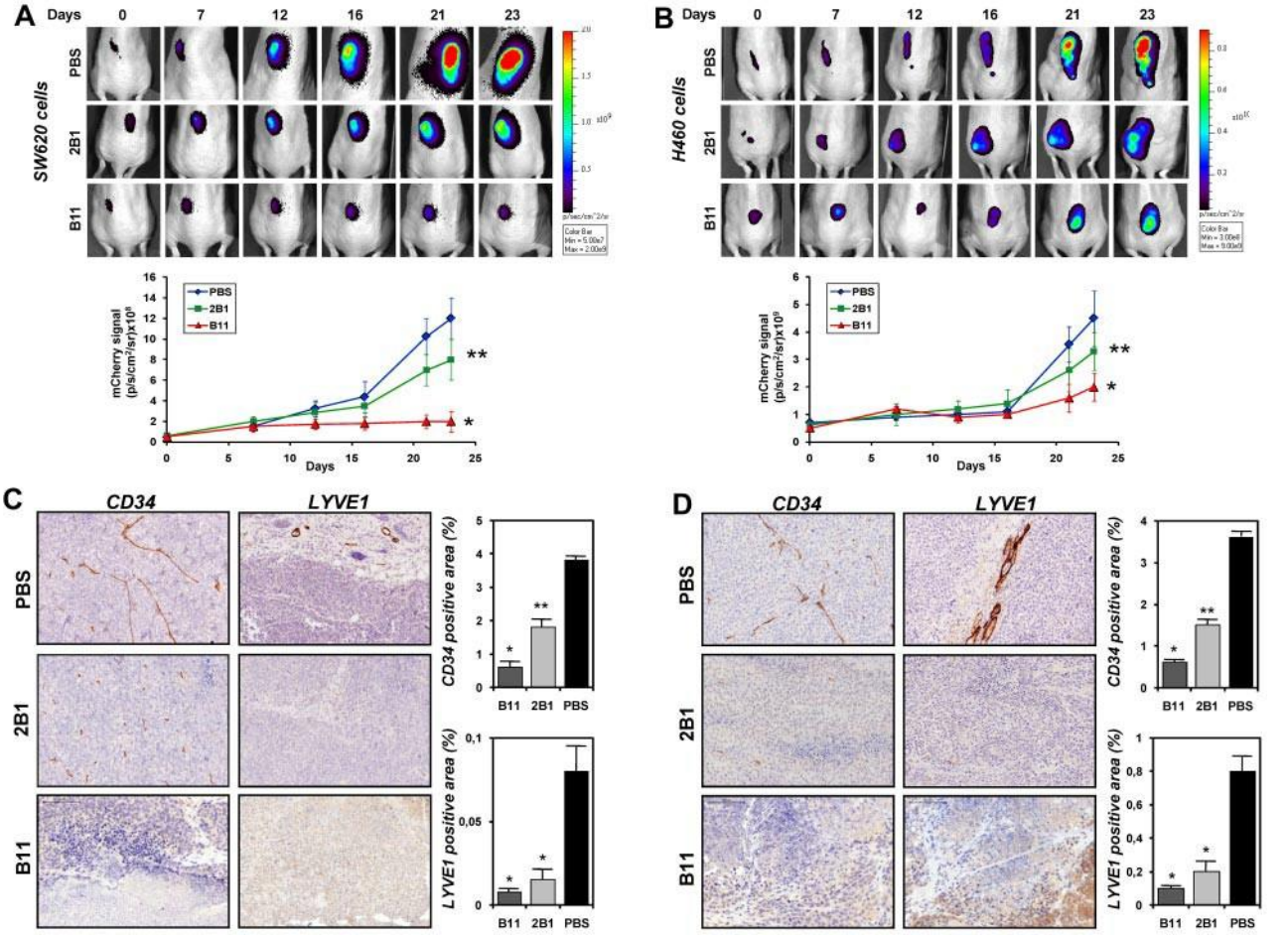

Figure 7. In vivo antitumor activity of the ephrinB2-specific scFvs on SW620 and H460 xenografts. (A) mCherry-expressing SW620 colon carcinoma cells (5 X 10^6) or (B) mCherry-expressing H460 lung carcinoma cells (5 X 10^6) were injected subcutaneously into *nu/nu* mice. Animals were noninvasively imaged for tumor growth at 610 nm using the IVIS Imaging System and were split into 3 groups for each experiment: control (n = 4), which received PBS injections, B11 (n = 4) and 2B1 (n = 4) groups that were injected IV with 20 mg/kg of the corresponding scFv on alternating days, starting at day 4 postimplantation. Representative dorsal images of treated and untreated mice at indicated times are shown. Quantitative assessments of the tumor photon counts of treated and untreated groups are shown in the lower panels. Error bars represent the SD; $*P < .001$, $**P < .01$. (C) Immunohistochemical staining on tumor sections from mice bearing SW620 or (D) H460 xenografts after treatment with PBS, 2B1, or B11. Blood vessel endothelial cells were stained with an anti-CD34 Ab (brown, endothelial cells; magnification, 200X) and lymphatic endothelial cells with an anti-LYVE-1 (brown, lymphatic endothelial cells; magnification, 200X). Representative photomicrographs of each experiment are shown. Quantification of the corresponding positive areas was performed with AxioVison software and plotted as percentage (mean ± SD) of the stained area relative to the total tumor area. $*P < .001$, $**P < .01$.

models of colorectal (SW620) and lung (H460) carcinoma cells in which the endogenous ephrinB2 levels substantially differed, suggesting that antitumoral activity was independent of the level of ephrinB2 expression in tumor cells. Actually, anti-ephrinB2 Abs failed to inhibit the growth of cultured BxPC3, SW620, and H460 cells, consistent with the hypothesis that anti-ephrinB2 scFvs affect tumor growth through an antiangiogenic mechanism rather than through inhibiting tumor cell proliferation per se. Therefore, the observed induction of apoptosis would be the consequence of eliminating blood vessels and reducing blood supply. The in vivo data presented herein also show that an effective inhibition of tumor lymphatic vasculature can be achieved by targeting ephrinB2 with specific Abs, indicating an important role for this molecule in the modulation of the lymphangiogenic process. Given that it has been extensively shown that the formation of lymphatic vessels into the tumor increases the capacity of tumors to metastasize,[41] it is tempting to speculate that the antilymphangiogenic activity of ephrinB2-specific Abs may restrain tumor spread by restricting tumor cell dissemination through the lymphatic vasculature. Further work will be needed to confirm this hypothesis.

Much remains to be learned about the mechanisms through which ephrinB2-specific scFvs inhibit angiogenesis and lymphangiogenesis . Recently, it has been demonstrated that ephrinB2 and VEGF signaling are mechanistically connected during both processes because ephrinB2 acts as a direct activator of VEGFR2 and VEGFR3 by controlling the internalization of both receptors.[19,20] EphrinB2 mutant with an impaired PDZ target site resulted in decreased filopodial extensions in endothelial tip cells as a consequence of failure to internalize VEGFR2. Furthermore, the tumor blood vessels in these mutant mice using an orthotopic glioma tumor model were characterized by a smooth and straight appearance lacking sprouts and filopodia.[19] Interestingly, we observed a comparable vascular phenotype in the blood vessels of tumors treated with anti-ephrinB2 Abs, suggesting that the binding of these scFvs would impair ephrinB2 reverse signaling through PDZ interactions and would inhibit the internalization of VEGFR2 and VEGFR3. Additional studies would be required to support this hypothesis.

In summary, we have described the generation and initial characterization of anti-ephrinB2 human scFvs that represent a new approach to target angiogenesis and lymphangiogenesis for cancer

treatment and, possibly, other angiogenesis-dependent pathologies. Targeting ephrinB2 with specific Abs significantly inhibited vascular organization and cell migration but not proliferation. Furthermore, scFv-treated HUVECs showed an abnormal motility characterized by a reduced velocity and a loss of directionality. Those effects may be regulated, at least in part, at the level of the cytoskeleton because treatment with anti-ephrinB2 Abs notably increased the formation of actin stress fibers. Moreover, these Abs were able to block physiologic angiogenesis and when administered to mice xenografted with different human tumor cells, they inhibited tumor progression by impairing tumor angiogenesis and lymphangiogenesis. In light of these results, B11 Ab may be suitable as a lead for the development of improved antiangiogenic therapies of application in cancer or other angiogenesis-based diseases. In the future, it will also be of interest to investigate whether anti-ephrinB2 Abs can complement or synergize with other established antiangiogenic agents.

Acknowledgments

The authors are grateful to Drs Keith Ashman, Fernando Pelaez, and Erwin Wagner for critical reading of the manuscript. They thank the staff of the Comparative Pathology and Flow Cytometry Units of CNIO for excellent technical support; and Diana Romero and Dr Luis Lombardía from the Molecular Diagnostics Unit of CNIO for advice on qRT-PCR experiments.

This work was supported by grants from the Regional Government of Madrid, Spain (Angiobodies Programmes, S-BIO-0236-2006 and S2010/BMD-2312).

Authorship

Contribution: M.A.A. designed and performed experiments, analyzed, and interpreted data; S.D.F. and A.R. acquired, analyzed, and interpreted in vitro data and revised the manuscript; S.F. contributed to the animal experiments; J.S., M.P.-M., and D.M. designed, performed, and analyzed data of confocal experiments; D.O. and S.O. performed animal experiments and revised the manuscript; M.M. performed Biacore experiments and analyzed data; M.C. analyzed and interpreted immunohistochemical data; and J.L.M.-T. designed research, analyzed and interpreted data, and wrote the manuscript.

Conflict-of-interest disclosure: The authors declare no competing financial interests.

The current affiliation for M.A.A. is Chemical and Physical Biology Department, Centro de Investigaciones Biológicas (CIB), Madrid, Spain. The current affiliation for S.d.F. is Physiology Department, Universidad de Alcalá, Madrid, Spain. The current affiliation for S.F. is Animal Facility, Faculty of Health Science, Universidad Rey Juan Carlos, Madrid, Spain.

Correspondence: Jorge L. Martínez-Torrecuadrada, Proteomics Unit, Biotechnology Programme, CNIO, Melchor Fernández Almagro 3, 28029 Madrid, Spain; e-mail: jlmartinez@cnio.es.

References

1. Risau W. Mechanisms of angiogenesis. *Nature.* 1997;386(6626):671-674.
2. Oliver G. Lymphatic vasculature development. *Nat Rev Immunol.* 2004;4(1):35-45.
3. Carmeliet P, Jain RK. Angiogenesis in cancer and other diseases. *Nature.* 2000;407(6801):249-257.
4. Carmeliet P. Angiogenesis in life, disease and medicine. *Nature.* 2005;438(7070):932-936.
5. Alitalo K, Tammela T, Petrova TV. Lymphangiogenesis in development and human disease. *Nature.* 2005;438(7070):946-953.
6. Ferrara N, Hillan KJ, Novotny W. Bevacizumab (Avastin), a humanized anti-VEGF monoclonal antibody for cancer therapy. *Biochem Biophys Res Commun.* 2005;333(2):328-335.
7. Sebolt-Leopold JS, English JM. Mechanisms of drug inhibition of signalling molecules. *Nature.* 2006;441(7092):457-462.
8. Dancey JE, Chen HX. Strategies for optimizing combinations of molecularly targeted anticancer agents. *Nat Rev Drug Discov.* 2006;5(8):649-659.
9. Jubb AM, Harris AL. Biomarkers to predict the clinical efficacy of bevacizumab in cancer. *Lancet Oncol.* 2010;11(12):1172-1183.
10. Paez-Ribes M, Allen E, Hudock J, et al. Antiangiogenic therapy elicits malignant progression of tumors to increased local invasion and distant metastasis. *Cancer Cell.* 2009;15(3):220-231.
11. Adams RH, Klein R. Eph receptors and ephrin ligands. essential mediators of vascular development. *Trends Cardiovasc Med.* 2000;10(5):183-188.
12. Makinen T, Adams RH, Bailey J, et al. PDZ interaction site in ephrinB2 is required for the remodeling of lymphatic vasculature. *Genes Dev.* 2005; 19(3):397-410.
13. Kullander K, Klein R. Mechanisms and functions of Eph and ephrin signalling. *Nat Rev Mol Cell Biol.* 2002;3(7):475-486.
14. Pasquale EB. Eph-ephrin bidirectional signaling in physiology and disease. *Cell.* 2008;133(1):38-52.
15. Himanen JP, Chumley MJ, Lackmann M, et al. Repelling class discrimination: ephrin-A5 binds to and activates EphB2 receptor signaling. *Nat Neurosci.* 2004;7(5):501-509.
16. Kalo MS, Yu HH, Pasquale EB. In vivo tyrosine phosphorylation sites of activated ephrin-B1 and ephB2 from neural tissue. *J Biol Chem.* 2001; 276(42):38940-38948.
17. Lin D, Gish GD, Songyang Z, Pawson T. The carboxyl terminus of B class ephrins constitutes a PDZ domain binding motif. *J Biol Chem.* 1999; 274(6):3726-3733.
18. Essmann CL, Martinez E, Geiger JC, et al. Serine phosphorylation of ephrinB2 regulates trafficking of synaptic AMPA receptors. *Nat Neurosci.* 2008; 11(9):1035-1043.
19. Sawamiphak S, Seidel S, Essmann CL, et al. Ephrin-B2 regulates VEGFR2 function in developmental and tumour angiogenesis. *Nature.* 2010;465(7297):487-491.
20. Wang Y, Nakayama M, Pitulescu ME, et al. Ephrin-B2 controls VEGF-induced angiogenesis and lymphangiogenesis. *Nature.* 2010; 465(7297):483-486.
21. Wang HU, Chen ZF, Anderson DJ. Molecular distinction and angiogenic interaction between embryonic arteries and veins revealed by ephrin-B2 and its receptor Eph-B4. *Cell.* 1998;93(5):741-753.
22. Gerety SS, Wang HU, Chen ZF, Anderson DJ. Symmetrical mutant phenotypes of the receptor EphB4 and its specific transmembrane ligand ephrin-B2 in cardiovascular development. *Mol Cell.* 1999;4(3):403-414.
23. Adams RH, Wilkinson GA, Weiss C, et al. Roles of ephrinB ligands and EphB receptors in cardiovascular development: demarcation of arterial/venous domains, vascular morphogenesis, and sprouting angiogenesis. *Genes Dev.* 1999;13(3): 295-306.
24. Yamanda S, Ebihara S, Asada M, et al. Role of ephrinB2 in nonproductive angiogenesis induced by Delta-like 4 blockade. *Blood.* 2009;113(15): 3631-3639.
25. Zheng W, Tammela T, Yamamoto M, et al. Notch restricts lymphatic vessel sprouting induced by vascular endothelial growth factor. *Blood.* 2011; 118(4):1154-1162.
26. Bochenek ML, Dickinson S, Astin JW, Adams RH, Nobes CD. Ephrin-B2 regulates endothelial cell morphology and motility independently of Eph-receptor binding. *J Cell Sci.* 2010;123(Pt 8):1235-1246.
27. Martiny-Baron G, Korff T, Schaffner F, et al. Inhibition of tumor growth and angiogenesis by soluble EphB4. *Neoplasia.* 2004;6(3):248-257.
28. Kertesz N, Krasnoperov V, Reddy R, et al. The soluble extracellular domain of EphB4 (sEphB4) antagonizes EphB4-EphrinB2 interaction, modulates angiogenesis, and inhibits tumor growth. *Blood.* 2006;107(6):2330-2338.
29. Martinez-Torrecuadrada J, Cifuentes G, Lopez-Serra P, Saenz P, Martinez A, Casal JI. Targeting the extracellular domain of fibroblast growth factor receptor 3 with human single-chain Fv antibodies inhibits bladder carcinoma cell line proliferation. *Clin Cancer Res.* 2005;11(17):6280-6290.
30. Adams RH, Alitalo K. Molecular regulation of angiogenesis and lymphangiogenesis. *Nat Rev Mol Cell Biol.* 2007;8(6):464-478.
31. Cristofaro B, Emanueli C. Possible novel targets for therapeutic angiogenesis. *Curr Opin Pharmacol.* 2009;9(2):102-108.
32. Krasnoperov V, Kumar SR, Ley E, et al. Novel EphB4 monoclonal antibodies modulate angiogenesis and inhibit tumor growth. *Am J Pathol.* 2010;176(4):2029-2038.
33. Koolpe M, Burgess R, Dail M, Pasquale EB. EphB receptor-binding peptides identified by phage display enable design of an antagonist

with ephrin-like affinity. *J Biol Chem.* 2005; 280(17):17301-17311.

34. Scehnet JS, Ley EJ, Krasnoperov V, et al. The role of Ephs, Ephrins, and growth factors in Kaposi sarcoma and implications of EphrinB2 blockade. *Blood.* 2009;113(1):254-263.
35. Chrencik JE, Brooun A, Kraus ML, et al. Structural and biophysical characterization of the EphB4*ephrinB2 protein-protein interaction and receptor specificity. *J Biol Chem.* 2006;281(38): 28185-28192.
36. Steinle JJ, Meininger CJ, Chowdhury U, Wu G, Granger HJ. Role of ephrin B2 in human retinal endothelial cell proliferation and migration. *Cell Signal.* 2003;15(11):1011-1017.
37. Toth J, Cutforth T, Gelinas AD, Bethoney KA, Bard J, Harrison CJ. Crystal structure of an ephrin ectodomain. *Dev Cell.* 2001;1(1):83-92.
38. Foo SS, Turner CJ, Adams S, et al. Ephrin-B2 controls cell motility and adhesion during blood-vessel-wall assembly. *Cell.* 2006;124(1):161-173.
39. Cowan CA, Henkemeyer M. The SH2/SH3 adaptor Grb4 transduces B-ephrin reverse signals. *Nature.* 2001;413(6852):174-179.
40. Keezer SM, Ivie SE, Krutzsch HC, Tandle A, Libutti SK, Roberts DD. Angiogenesis inhibitors target the endothelial cell cytoskeleton through altered regulation of heat shock protein 27 and cofilin. *Cancer Res.* 2003;63(19):6405-6412.
41. Cassella M, Skobe M. Lymphatic vessel activation in cancer. *Ann N Y Acad Sci.* 2002;979:120-130.